frontiers | Frontiers in Materials

TYPE Original Research
PUBLISHED 20 December 2023
DOI 10.3389/fmats.2023.1260609

OPEN ACCESS

EDITED BY
Naveed Afzal,
Government College University, Lahore, Pakistan

REVIEWED BY
Lakshmi Narayanan Mosur Saravana Murthy,
Intel, United States
Shihui Yu,
Tianjin University, China

*CORRESPONDENCE
Muhammad Shafiq Anjum,
shafiqanjum55@gmail.com
Muhammad Waseem Ashraf,
dr.waseem@gcu.edu.pk

RECEIVED 18 July 2023
ACCEPTED 01 November 2023
PUBLISHED 20 December 2023

CITATION
Anjum MS, Ashraf MW, Tayyaba S and Imran M (2023), Simulation, synthesis, and analysis of strontium-doped ZnO nanostructures for optoelectronics and energy-harvesting devices.
Front. Mater. 10:1260609.
doi: 10.3389/fmats.2023.1260609

Simulation, synthesis, and analysis of strontium-doped ZnO nanostructures for optoelectronics and energy-harvesting devices

Muhammad Shafiq Anjum[1]*, Muhammad Waseem Ashraf[1]*, Shahzadi Tayyaba[2] and Muhammad Imran[1]

[1]Department of Electronics, Institute of Physics, Government College University, Lahore, Pakistan, [2]Department of Information Sciences, Division of Science and Technology, University of Education, Lahore, Pakistan

The demand for clean and sustainable alternative energy resources is linearly increasing day by day due to the prevailing electricity crisis. Small-scale energy harvesting is considered a sustainable way to generate clean energy. Advanced energy solar cells, mainly dye-sensitized solar cells use solar energy and convert it into electrical energy. Similarly, MEMS-based piezoelectric materials are used to convert mechanical energy into electrical energy. For these applications, zinc oxide is considered one of the most suitable materials with high conductive, tunable band gap, and piezoelectric properties. However, altering these properties can be carried out by the addition of metal and other materials. Various research work has been carried out to study the addition of conductive metal as a dopant to alter the properties of zinc oxide. In this study, Strontium has been doped in ZnO to form a nanostructure for application in DSSC and microelectromechanical systems (MEMS) energy harvesters. Analysis has been conducted using the simulation and fabrication method. The results show that the doping and the pore size of the substrate (Anodic Aluminum oxide membrane) largely affect the output voltage and current. The difference between the simulated and experimental results was less than 1%, which shows the accuracy of the simulation. Tuning of the band gap can be observed by the addition of Sr in the ZnO nanostructure. For microelectromechanical systems energy harvesters, Sr-doped ZnO nanostructures deposited on anodic aluminum oxide show 7.10 mV of voltage and 1.11 uA of current output. The addition of Sr doping in ZnO shows the improvement in the generated current and voltage for the energy harvester and the improvement in overall power conversion efficiency for dye-sensitized solar cells. MEMS-based energy harvesting devices and low-cost advanced solar cells are promising to improve the efficiency of energy generation at a small scale.

KEYWORDS

opto-electronic devices, energy harvesters, strontium, zinc oxide, DSSC, dye, nanorods

1 Introduction

The intensifying energy crisis and increasing electricity costs and their hazardous impact on the environment have attained a substantial amount of attention in research and development due to the requirement for more efficient and viable alternative energy resources (Chakraborty et al., 2021). This makes renewable and energy harvesting systems a necessity for addressing the energy crisis around the globe. Energy harvesting can be performed from various techniques and sources, depending on the type of technology used to generate the clean energy, and includes thermoelectric energy harvesting, photovoltaic energy harvesting, piezoelectric energy harvesting, pyroelectric energy harvesting, electromagnetic energy harvesting, wind energy harvesting, and vibration energy harvesting (Davidson and Mo, 2014; Akinaga, 2020; Zhou et al., 2021). Solar energy generation has gained momentum in the last few decades due to its higher efficiency and high availability. However, the associated cost of solar panels makes it a less cost-effective energy generation method (Pastuszak and Węgierek, 2022). This opens up an opportunity for low-cost advanced-generation solar cells, which are currently being synthesized in laboratories and are considered to be the future of low-cost and efficient solar energy generation. Organic solar cells, perovskite solar cells, and dye-sensitized solar cells (DSSCs) are considered the future of the solar cell industry. However, the high cost of perovskite materials, stability issues, and low lifetime of organic and perovskite solar cells are considered the biggest drawbacks of these solar cells. Among these solar cells are dye-sensitized solar cells, which are easy to fabricate, low-cost flexible, lightweight, and reliable solar cells. DSSCs are gaining momentum due to their capability of efficiency improvement by modification of their cell layers (Alizadeh et al., 2022). Currently, the highest reported efficiency of DSSCs is 14.1% but researchers are working towards improving the efficiency with easy fabrication techniques and low cost of cell preparation (Singh and Shougaijam, 2022). The efficiency of energy conversion in a dye-sensitized solar cell is determined by the semiconductor, sensitizer, electrolyte, and counter electrode. The efficiency of DSSCs can be improved by carefully determining the optimal importance of several manufacturing process factors (Castán et al., 2022; Richhariya et al., 2022; Ari et al., 2023). ZnO-based semiconductor photo anode has been used in DSSCs under different morphologies including nanoparticles, nanorods, and nanowires. Chung et al. reported that an improvement in the fill factor of the DSSC is observed when annealed nanorods are used as photoanodes due to better crystallinity (Chung et al., 2010). Similarly, a power conversion efficiency of 2.35% has been reported using hedgehog-like ZnO-nanorods on the ZnO nanoparticle seed layer (Yuliasari et al., 2022). Moreover, several doped ZnO nanostructures are reported in the literature as photoanodes for DSSCs with improved photovoltaic efficiencies. For example, Cd-doped ZnO nanostructures show a power conversion efficiency of 0.5%, Cu-doped ZnO nanostructures show a power conversion efficiency of 2.03%, and Pd-doped ZnO nanostructures show a power conversion efficiency of 11.92% (Esgin et al., 2022; Esakki et al., 2023; Mujahid and Al-Hartomy, 2023). However, the study of the second group of highly conductive metals and their doping with ZnO has not been reported in the literature. Since the second group elements are extremely stable and conductive, they are considered an excellent additive in ZnO nanocrystals for the improvement of the efficiency of solar cells.

On the other hand, microelectromechanical systems (MEMS)-based energy harvesters have been used due to their small size and complete package on a single chip (Fang et al., 2006; Zorlu et al., 2013; Sun et al., 2018; Toshiyoshi et al., 2019). MEMS-based energy harvesters have advantages over the conventionally used systems, including low cost, easy maintenance, relatively easier operation, higher efficiency, low environmental impacts, easier synthesis and fabrication, and wireless systems for better usage (Liu et al., 2012; Bounouh and Bélières, 2014). These devices use ambient mechanical energy, converting it into useful electrical energy. Among different types of MEMS-based energy harvesting, piezoelectric energy harvesters utilize mechanical energy in the form of stress and pressure and convert it into electrical energy. The mechanical energy applied can be in the form of stress including vibrational stress, noise, strain, sonic waves, applied temperature gradient, energy generated due to gas and liquid flow as well as other physical motions (Rajeev et al., 2021). Different MEMS-based energy harvesters, including triboelectric nanogenerators and piezoelectric nanogenerators, have gained popularity in terms of generating clean energy (Maamer et al., 2019; Anand et al., 2021; Zhang et al., 2021). Among these devices, piezoelectric nanogenerators use piezoelectric materials that are capable of converting mechanical energy (vibration and stress) into useful electrical energy. Some useful and commonly used piezoelectric materials include zinc oxide (ZnO), lead zirconate titanate, barium titanate, lead titanate, and lithium tantalite (Bestley Joe and Shaby, 2021; Iqbal et al., 2021; Poon et al., 2021; Tiwari et al., 2021; Debnath and Kumar, 2022). ZnO has been considered as the most suitable material piezoelectric energy harvester (Karumuthil et al., 2019; Rajeev et al., 2020). ZnO exhibits excellent band gap tenability and piezoelectric properties owing to its structural properties of transparency, n-type dipole structure for cutting-edge piezoelectric properties, its ability to alter nanostructural properties, and its chemical stability as well as no lead-based toxic impurity, which damages energy harvesters (Gullapalli et al., 2010; Vaseem et al., 2010; Cherumannil Karumuthil et al., 2017). With these excellent properties, ZnO has been extensively used as a piezoelectric MEMS energy harvester. Tao reported the use of ZnO as a 2DOF MEMS energy harvester with a reported voltage output of 10 and 15 mV (Tao et al., 2019). Similarly, Wang reported the use of dual ZnO thin film with a highly improved voltage output of 1.77 V. The research was performed with ANSYS simulation and the accuracy of the simulation still needs to be checked (Wang and Du, 2015a). Doped ZnO nanostructures for application in MEMS energy harvesters still require further research to study their impact on the current density and voltage output.

Owing to the superior properties of ZnO, the structural and optical properties of ZnO can be altered by doping it with other materials. The group II elements, including calcium, magnesium, strontium, and barium, are considered the most conductive materials that can be easily incorporated into the atomic structure of ZnO, resulting in altered structural and optical properties, including the grain size and band-gap, of ZnO structures produced as a result of doping (Sheikh et al., 2013; Afzal et al., 2020; Baig et al., 2020; Sarwar et al., 2021). Adding second group element doping in ZnO nanostructures results in the alternation of the band gap as well as the structural morphology of ZnO nanostructures (Mahdhi et al., 2018; Sarwar and Ashraf, 2020; Tayyaba et al., 2020). Various ways can be

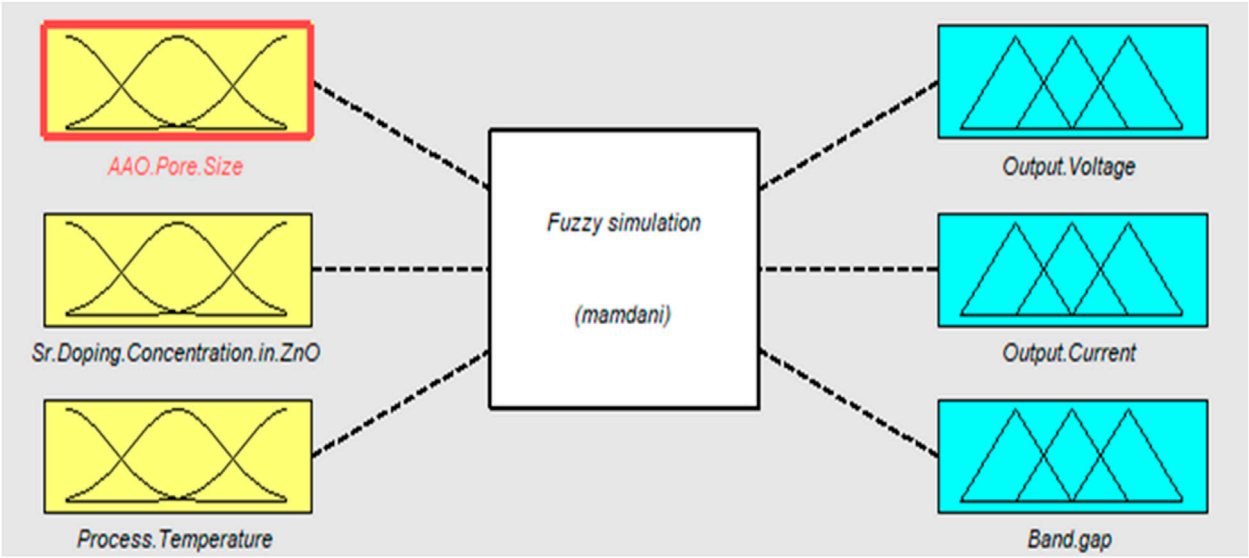

FIGURE 1
FIS model for simulation.

used to prepare the ZnO nanostructures including chemical and physical methods (Dobrzański and Pakuła, 2005; An et al., 2020; Boing et al., 2020). The chemical techniques are considered low-cost techniques; however, their reproducibility is relatively lower as compared to physical techniques. Among different chemical techniques, chemical bath deposition is considered one of the most efficient methods to generate ZnO thin film with different types of nanostructures (Wu and Liu, 2002; Hodes, 2007; Mugle and Jadhav, 2016; Wasim et al., 2020).

There is a research gap that lies within the study of the small-scale energy harvesting methods (DSSCs and MEMs energy harvesters) fabricated using second group element doped ZnO. Among second group elements, including Mg, Ca, Be, and Sr, Strontium has a similar ionic radius to zinc, which minimizes lattice distortion and defect formation, leading to enhanced electrical properties in ZnO. As the ionic radius of strontium is large as compared to the other elements of group II, it is expected to alter the properties of ZnO more as compared to other group elements including Mg and Ca. Whereas Mg, Ca, and Be doping can introduce more significant lattice disruptions and defects due to differences in ionic radii. In this study, simulation and experimental work related to strontium-doped ZnO has been conducted for use in a dye-sensitized solar cell and MEMS energy harvester. The study included the fabrication of an anodic aluminum oxide (AAO) template, which was used as a substrate. The optical, structural, photovoltaic, and piezoelectric properties of Sr-doped ZnO nanostructures were analyzed. We have conducted a comparative study between solar cell and MEMS energy harvesting by developing complete solar cell and MEMS-based energy harvesters based on Sr-doped ZnO nanostructures and predicting the voltage and current of the energy harvesters.

2 Fuzzy analysis

A fuzzy rule-based system was used to predict the voltage and current output of the ZnO used as an anode of solar cells and the piezoelectric material in energy harvesters. Anodic aluminum oxide was used as a template, and Sr-doped zinc oxide nanostructures were deposited on the substrate to study energy generation properties. Figure 1 shows the fuzzy logic interface for the simulation. The input used includes anodic aluminum oxide pore size, Sr doping concentration in zinc oxide, and the process temperature for the deposition of the Sr-doped ZnO nanostructures. The band gap of the prepared film, current, and voltage for the energy harvesters were taken as output.

Based on the literature, the ranges of the input and output parameters were selected in order to predict the possible solution for the output of the energy harvesters. The input pore size of the AAO membrane varied from 1 to 1,000 nm, the Sr-doping concentration in ZnO ranged from 2% to 8%, and the process temperature for the process varied from 10 to 95°C. The output parameters were assigned the ranges of 2–8 mV for output voltage, 0.3–1.8 uA for output current, and 3.1–3.4 eV for band gap value. The rules were then selected based on real life scenarios and the literature. A total of 27 rules were selected and based on these rules, a rule viewer graph was studied and analyzed with the variation of inputs. The rule viewer result was then compared with the Mamdani model. Calculated values were compared for error between the simulated and calculated values.

Figure 2 shows the rule viewer of the inputs and outputs based on the rules selected. It was observed that at an AAO membrane with a pore size of 300 nm, with 4% doping of Sr in ZnO nanostructures, and at 90°C process temperature, generated an output voltage of 7.08 mV, an output current of 1.12 uA, and a band gap of 3.25 eV, as shown in Figure 2.

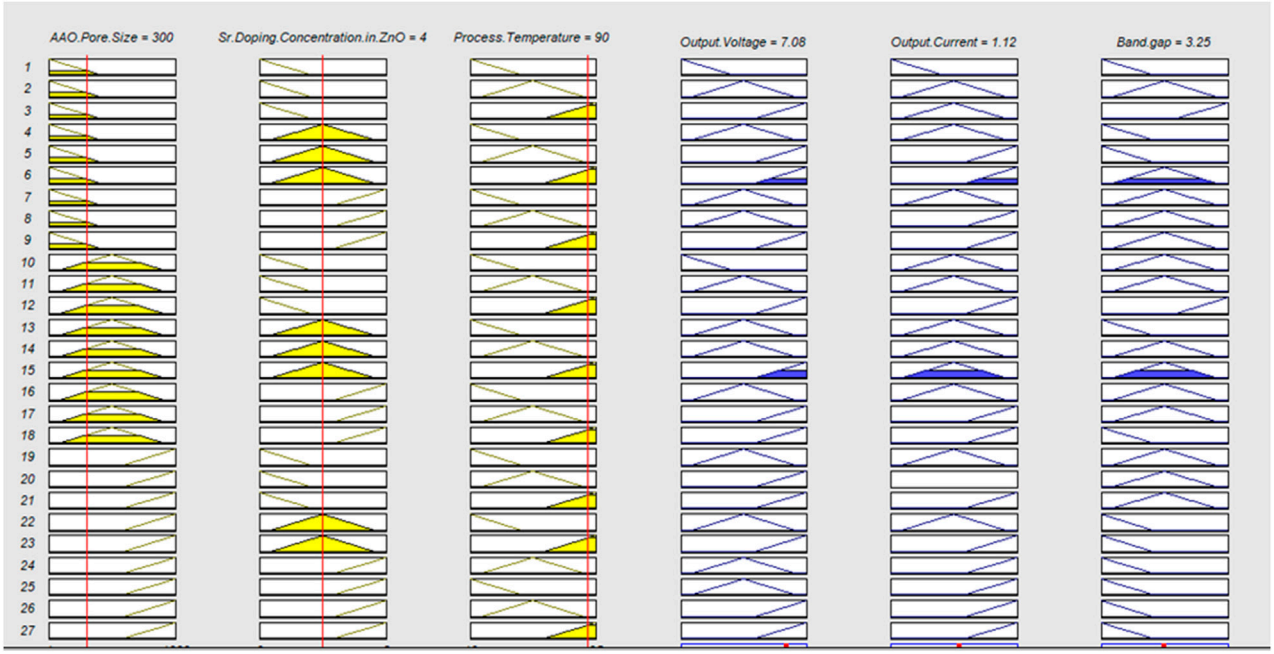

FIGURE 2
Rule viewer of the Fuzzy simulation.

TABLE 1 Differences between the simulated and calculated values for the fuzzy simulations.

	Simulated value	Calculated values	Error (%)
Output Voltage	7.08 mV	7.10 mV	0.28
Output Current	1.12 uA	1.10 uA	1.7
Band gap	3.25 eV	3.24 eV	0.2

Based on the simulated values from the rule viewer, the values were compared with the Mamdani calculated values using the Mamdani model formula as shown below in Equation 1.

$$P=\left[\frac{\sum(Ri\ x\ Si)}{\sum Ri}\right] \quad (1)$$

where Ri is equal to the minimum membership function value and Si is known as the singleton value.

The differences between the simulated and calculated values along with the differences between the values are shown in Table 1. The values show that the simulated and calculated values had a very small error that led to the accuracy of the designed system.

3 Materials and methods

All materials were analytically cleaned. The synthesis of Sr-doped ZnO nanostructure with 4% doping was performed on the anodic aluminum oxide substrate. The porous anodic aluminum oxide substrate was fabricated via an anodization process that is similar to an electrochemical system. The Sr-doped ZnO nanorods were then deposited on the porous AAO substrate. Then, contacts were sputtered on the designed MEMS energy harvester to analyze the current and voltage of the energy harvester. The Pt counter electrode, dye, and electrolyte were used for solar cells, and a solar simulator was used for the complete solar cell analysis.

3.1 Fabrication of the AAO template

An aluminum substrate with a 4 cm × 4 cm dimension was initially cleaned and pretreated using acetone and isopropyl alcohol to remove impurities. After cleaning, the substrate was subjected to electropolishing for the smoothing of the substrate's surface. After electropolishing, the substrate was again cleaned and sonicated to prepare it for anodization. Anodization of the aluminum was carried out in two different steps, namely, mild and hard anodization. In both steps, the anode was the aluminum substrate with the lead rod as the cathode and 0.5 M oxalic acid as the electrolyte. Hard and mild anodization steps were different in the following ways,

1) Initially, the mild anodization was carried out at 45 V for 30 min. After 30 min the voltage was increased to 130 V in small intervals and sustained at 130 V for 10 min followed by etching of the sample with chromic acid at a temperature less than the boiling point of water.
2) In the hard anodization step, the same process of mild anodization was carried out at 120 V for 4 h. The barrier layer created was removed by changing the electrolyte to potassium chloride (KCL) solution with opposite anode and cathode polarity for 6 min followed by etching in order to remove any impurities.

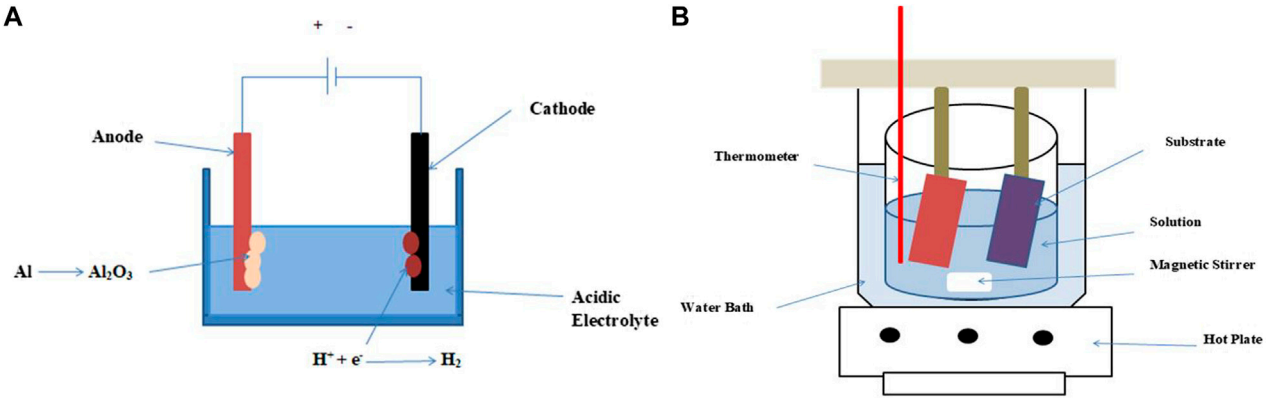

FIGURE 3
Process of **(A)** Anodization **(B)** Chemical bath deposition.

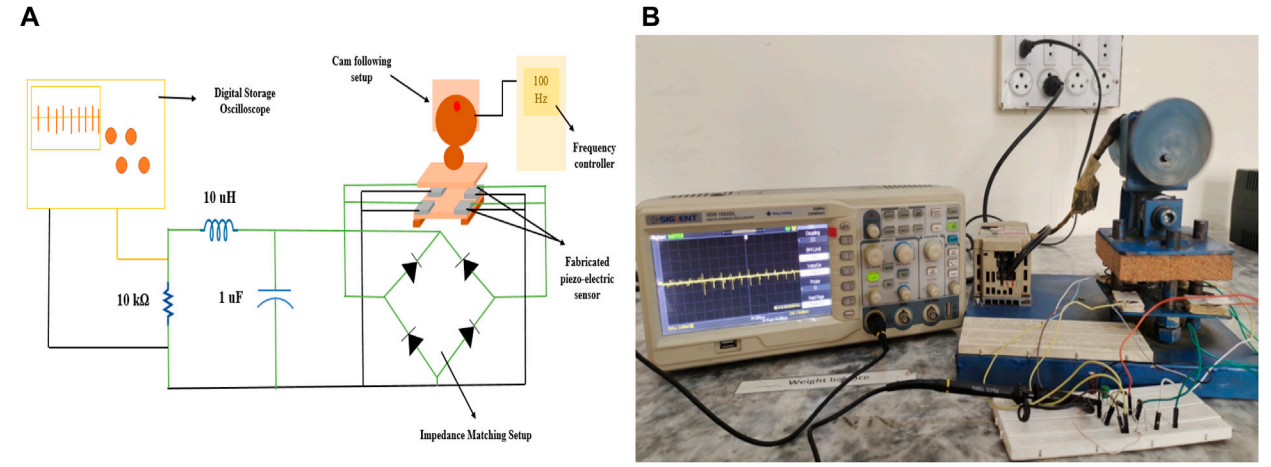

FIGURE 4
The output setup to monitor the voltage and current output **(A)** Block diagram **(B)** Implemented circuit.

The prepared anodic aluminum oxide membrane was then characterized using a scanning electron microscope and used as a template for the growth of Sr-doped ZnO nanostructures.

3.2 Fabrication of Sr-doped ZnO nanostructures

For the growth of Sr-doped ZnO nanostructures on the AAO template, zinc acetate di-hydrate and strontium acetate were used as the precursor. Then, 4% strontium acetate was added to the 20 mM solution of zinc acetate di-hydrate, and a hexa-amine solution was prepared in distilled water to make the solution for the chemical bath deposition. The prepared AAO template was then subjected to the process of chemical bath deposition, in which the template was vertically immersed into the prepared solution for 6 h at 90°C (process temperature selected in the fuzzy rule-based system). The solution was changed after every 3 h. The prepared film was then washed with distilled water and subjected to annealing at 400°C to prepare aligned nanorods of Sr-doped ZnO. The electrodes were then sputtered off the film to further test it for the voltage and current.

The process of anodization and chemical bath deposition is shown in Figure 3.

3.3 Characterization

The prepared samples were characterized in order to check structural and optical properties along with their energy harvesting properties. The structure of the prepared AAO template and the Sr-doped ZnO was characterized using a scanning electron microscope, the phase identification was carried out using x-ray diffraction. The optical properties were studied using UV-VIS spectrometry and the band gap was calculated.

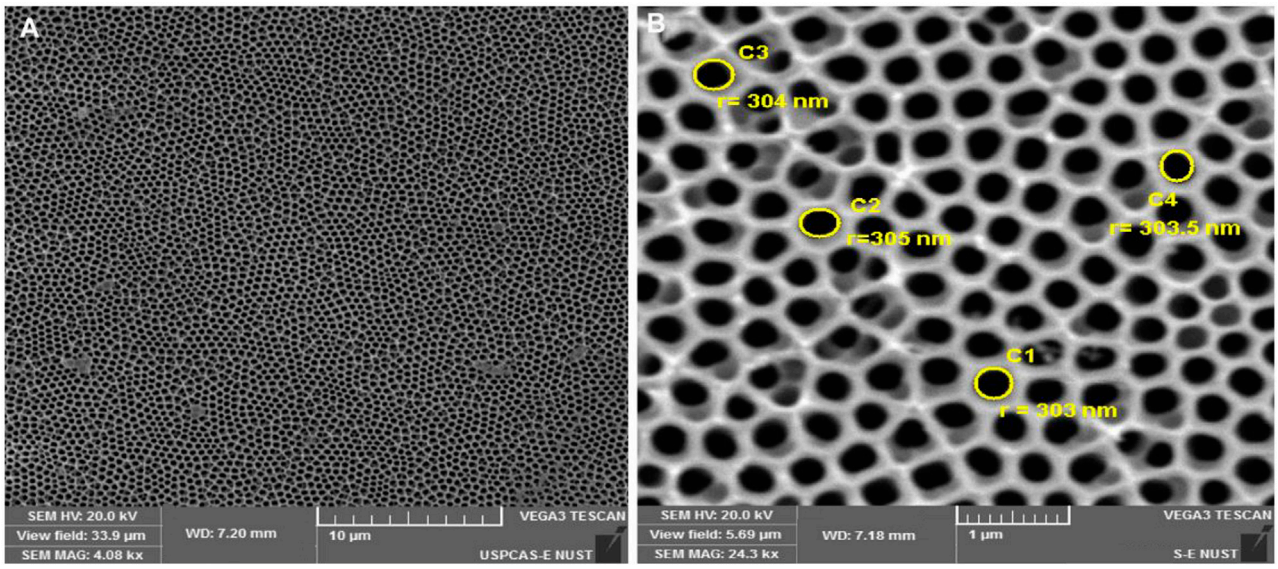

FIGURE 5
SEM results of the porous anodic aluminum oxide membrane **(A)** 10 µm **(B)** 1 µm.

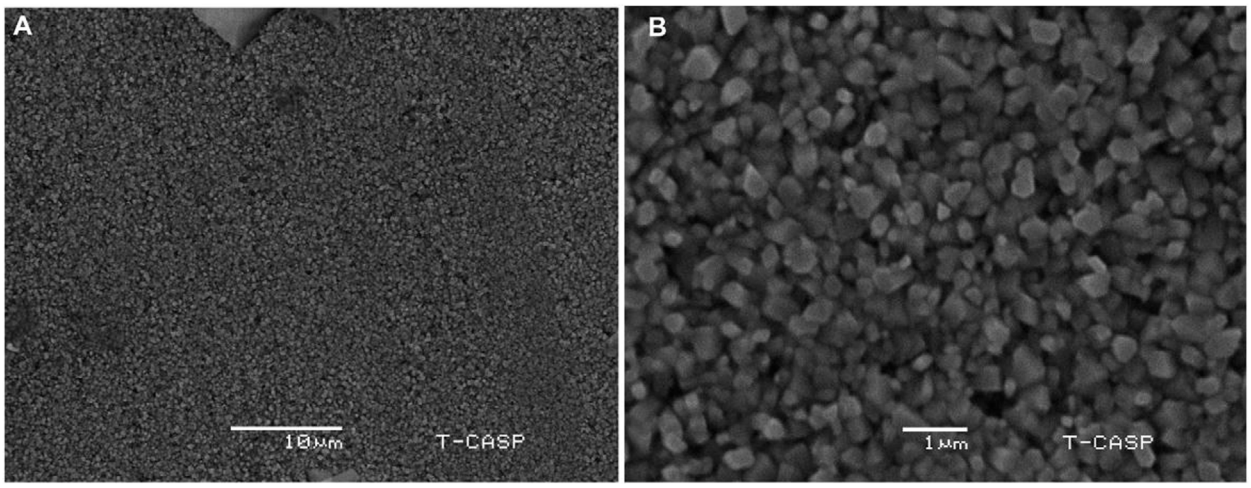

FIGURE 6
SEM results of the Sr doped ZnO nano-structures **(A)** 10 µm **(B)** 1 µm.

3.4 Designing a dye-sensitized solar cell

For the device fabrication, the prepared anode on the AAO membrane was dipped into an N3 dye solution for 20 h to improve dye absorption. As a counter electrode, ITO glass with a thin coating of gold was utilized. The photo-anode containing dye was clipped with the gold counter electrode. Using capillary action, a redox electrolyte (I-/I-3) solution was introduced into the gap between the electrodes. To test the repeatability of the produced Sr-doped ZnO on the AAO membrane, three sets of cells were made. A potentiostat system (Biological VSP) with a working distance of 8 cm and light intensity similar to that of the Sun was used for IV measurements.

3.5 MEMS piezoelectric energy harvester

The voltage and current of the MEMS energy harvester were analyzed by using a cam follower system and the SIGLENT SDS 1052DL oscilloscope. Three sets of samples were prepared. The sample, along with the electrodes, were placed in a plastic casing in

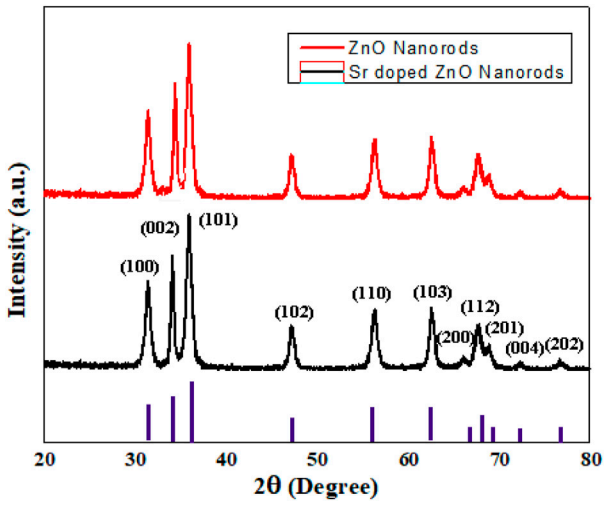

FIGURE 7
X-ray diffraction of the prepared Sr-doped ZnO nanorods on the AAO template.

between two stages of the cam follower. The frequency of the cam follower system could be controlled with frequency derived that was connected to a rotating system. The device was placed in between a fixed and movable stage. The movable stage moved with respect to the selected frequency. With every rotation, pressure was applied to the film, resulting in the generation of voltage and current, which was monitored by using the SIGLENT SDS 1052DL oscilloscope, and it was connected to the computer to analyze the current and voltage curves. An impedance matching circuit was added in between the energy harvester output and the measuring device in order to generate optimum output with load matching to achieve maximum power. The block diagram and the designed setup to study the piezoelectric energy harvesting output current and voltage are shown in Figure 4.

4 Results and discussion

4.1 Structural analysis

The structural properties of the AAO membrane were analyzed using the scanning electron microscope. Figure 5 shows the scanning electron microscope images. It was observed that nanopores were uniformly distributed throughout the template with hexagonal geometry. Due to the high voltage and large time of the anodization process, smoother and more uniform nano-porous geometry was observed (Michalska-Domańska et al., 2013). The pore size of the hexagonal porous in the range of 302–311 nm was observed.

Figure 6 shows the scanning electron microscope results of Sr-doped ZnO nanorods prepared by using the chemical bath deposition method. The prepared films were magnified and studied at two different magnifications, 1 and 10 um. The SEM micrographs clearly showed the growth of dense vertically aligned nanorods of Sr-doped ZnO nanostructures. The diameters of the prepared nanorods ranged from 300 to 350 nm. Since the nanorods grew on the highly porous AAO structure, the root cause of aggregation of the ZnO nanorods was reduced, and the prepared nanorods grew vertically with hexagonal morphology (Choi et al., 2015).

The rod diameter and the pore size of the AAO membrane were almost similar, providing a suitable substrate for the growth of properly aligned Sr-doped nanorods.

4.2 Phase analysis

The X-ray diffraction result for the prepared Sr-doped ZnO nanostructure of the AAO template is shown in Figure 7. The

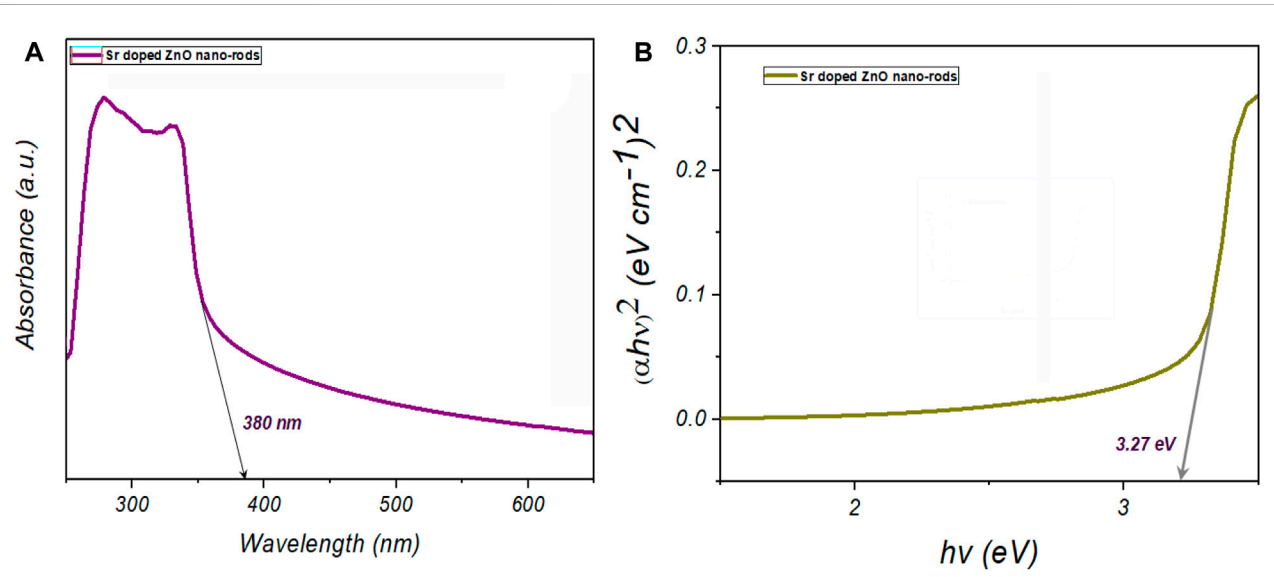

FIGURE 8
UV-vis study of the prepared Sr-doped ZnO nanostructures **(A)** absorption spectra **(B)** band gap Tauc plot.

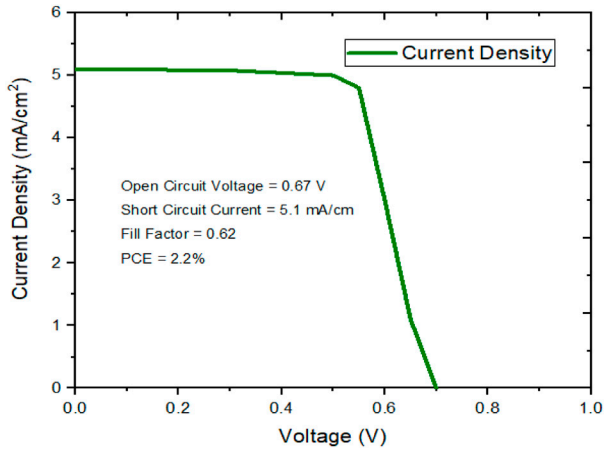

FIGURE 9
IV characteristic for the Sr-doped ZnO nanorods on the AAO substrate as anode.

graphs clearly show the formation of hexagonal wurtzite ZnO structures as per the JCPDS card number 89–1,397, along with a few major peaks at (100), (002), (101), (102), (110), and (103). The presence of the broader peaks of (002) and (101) clearly depicts the vertical c-axis direction of the nanostructure formed. However, based on the incorporation of Sr doping in the ZnO nanocrystal, no significant peak was observed in the spectra, and no change in the structural morphology was observed except for a small shift in the (002) peak. The shift towards the positive and higher values of the 2Θ was mainly due to the instability of its intensity and based on the up and down behavior of the change of the crystallinity of ZnO due to the addition of Sr in the ZnO nanostructure. The prepared Sr-doped ZnO nanorods, however, are immune to a reduction in oxygen vacancies, lattice distortion, and density defects as compared to conventionally used ZnO nanorods (Vijayan et al., 2008; Yarahmadi et al., 2021).

4.3 Optical analysis

The optical properties of the prepared ZnO nanostructures were observed using the UV-vis spectrophotometer. Figure 8A shows the absorbance spectra of the prepared Sr-doped ZnO nano-structure in the wavelength range of 250–650 nm. With the addition of almost similar ionic radii elements to the crystal structure of ZnO, a slight blue shift was observed as compared to the conventional system. The approximated band gap of the prepared sample was calculated by drawing a tangential line, as shown in Figure 8A. For the estimation of the band gap, we plotted a Tauc plot, as shown in Figure 8B. A change in the band gap was observed from the pure ZnO nanostructure due to the blue shift observed in the absorbance graph. The band gap was decreased due to the addition of a high atomic size element (Sr) into the ZnO nanostructures. The Fermi level rose into the

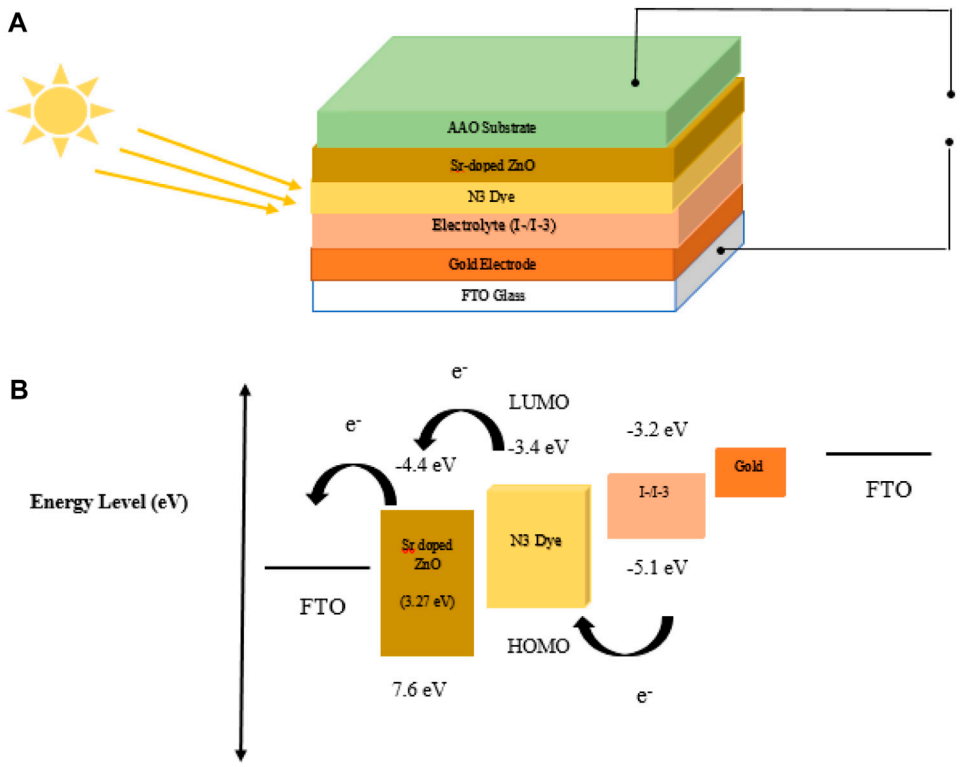

FIGURE 10
(A) Proposed dye-sensitized solar cell using Sr-doped ZnO photoanode **(B)** Energy band diagram of dye-sensitized solar cell using Sr-doped ZnO photoanode.

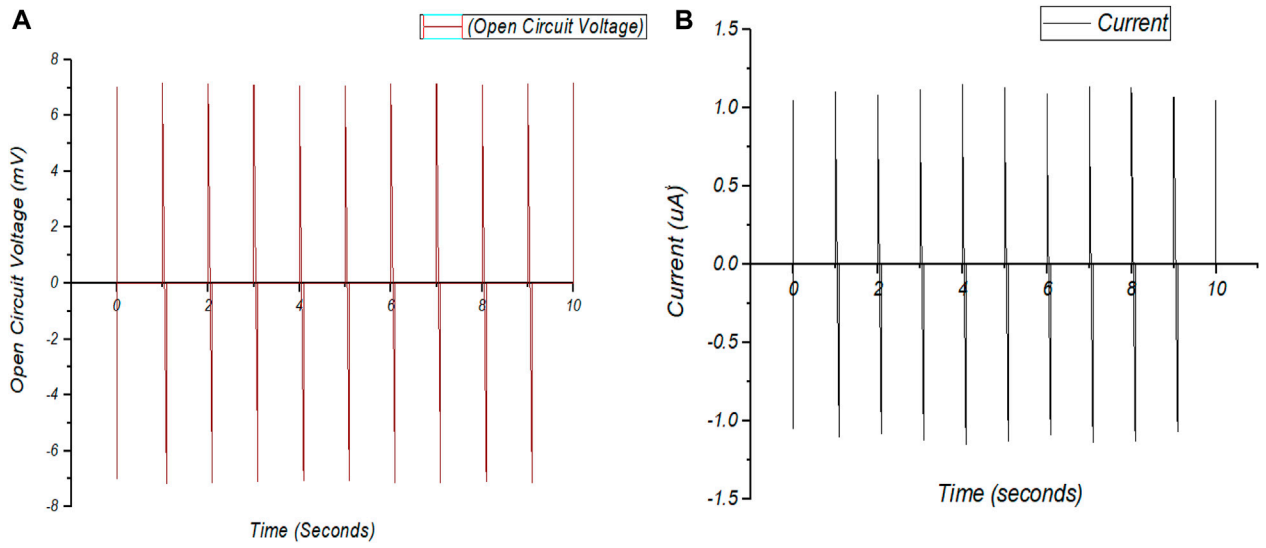

FIGURE 11
The IV characteristic curves of the energy harvester **(A)** open circuit voltage **(B)** short circuit current.

TABLE 2 Comparison of simulated and experimental results.

	Simulated results	Experimental result
Output Voltage	7.08 mV	7.10 mV
Output Current	1.12 uA	1.15 uA
Band gap	3.25 eV	3.27 eV

conduction band with the addition of a dopant. Conduction band filling causes absorption transitions to occur between the valance band and Fermi level rather than the valance band and the bottom of the conduction band. This shift in the absorption energy levels causes the energy band to widen (Eg) and the absorption edge to move to higher energies (Vijayan et al., 2008). The calculated band gap of the Sr-doped ZnO nanostructure was calculated to be 3.27 eV as compared to 3.25 eV of pure ZnO nano-structures, which is in accordance with the fuzzy logic rule-based system.

4.4 Photovoltaic analysis of dye-sensitized solar cell

The influence of Sr-doped ZnO on the AAO membrane on DSSC photovoltaic performance was investigated. The V_{oc} and J_{sc} were used to compute the fill factor and efficiency of the prepared cell. The overall IV properties of the Sr-doped ZnO on the AAO template as a working electrode demonstrated superior charge transfer and transfer for electron transport across the circuit, as illustrated in Figure 9. The device's performance was measured at 2.2% conversion efficiency, 0.67 V open circuit voltage, 5.1 mA/cm^2 short circuit current density, and 0.62 fill factor. Due to differences in the substrate for both the anode and cathode in the DSSC device, an uncomfortable sealing method may induce short-circuit effects between the anode and cathode. Furthermore, the device's performance was characterized by a decrease in open circuit voltage fill factor and short current density. The overall fabricated solar cell and its band diagram are shown in Figures 10A, B.

4.5 MEMS piezoelectric energy harvester analysis

The voltage and current generated by the energy harvesting system were analyzed using the cam follower system and the SIGLENT SDS 1052DL oscilloscope. The open circuit voltage and short circuit current, as shown in Figure 11, were measured under both the polarities when the pressure was applied as well as when the pressure was removed. The measured open circuit voltage fell in the range of 7.0–7.2 mV and the short circuit current fell in the range of 1.05–1.15 uA in terms of both polarities. The results of the voltage and current were also in accordance with the fuzzy rule-based system. It was observed that the results of open circuit voltage improved for the energy harvester as compared to ZnO energy harvesting systems. The voltage and current also depended on the growth of the vertically aligned Sr-doped ZnO nanostructures. The highly vertically aligned nanorods result in a higher generation of energy (Ali et al., 2019).

Table 2 shows the comparison between the simulated results from the fuzzy rule-based system and the experimentally calculated output. The simulated and experimental results were in close agreement with each other with a very small error.

The reported study with Sr-doped ZnO nanorods on an AAO template showed an improvement in the overall power conversion efficiency of the dye-sensitized solar cell as compared to the conventionally used solar cell with ZnO nanorods. The comparative study of the ZnO nanorods and doped ZnO nanorods is shown in Table 3. Sr-doped ZnO showed power conversion efficiency improvement as compared to conventional ZnO nanorods because of the increase in the band gap of the material, which resulted in easy

TABLE 3 Benchmark of the dye-sensitized solar cells.

References	Photoanode material	Band gap (eV)	V_{oc} (V)	J_{sc} (mA/cm^2)	Fill Factor	PCE (%)
Yuliasari et al. (2022)	ZnO nanorods grown using ZnO nanoparticles seed layer	—	0.67	7.06	0.49	2.35
Esgin et al. (2022)	Cu-doped ZnO nanopowder	3.28	0.61	5.96	0.43	2.03
Esakki et al. (2023)	Cd-doped ZnO	2.48	0.6	2	0.425	0.5
Selva Esakki et al. (2022)	Mg-doped ZnO	3.51	0.56	6.08	0.50	1.72
Rathnasekara and Hari (2022)	Ag-doped ZnO	3.22	0.58	19.12	0.55	1.45
Present study	Sr-doped ZnO on an AAO template	3.27	0.67	5.1	0.62	2.2

TABLE 4 Benchmark table for MEMS energy harvesters.

References	Piezoelectric material	Open circuit voltage (V_{oc}) (mV)	Short circuit current (J_{sc}) (uA)
Ali et al. (2019)	ZnO nanostructure on an AAO template	3–6.4	0.45–1.5
Tao et al. (2019)	ZnO thin films for 2DOF	10–15	—
Wang and Du (2015b)	Dual ZnO piezoelectric element	2.06	—
Md Ralib et al. (2012)	Al-doped ZnO thin film	1.61	—
Zhao et al. (2019)	Li-doped ZnO thin film	10.2	—
Present study	Sr-doped ZnO on an AAO template	7.0–7.2	1.05–1.15

transport of electrons generated in the dye to the external circuit. Similarly, the porous structure of the AAO template facilitated the movement of electrons. Table 3 shows that as compared to other metal-doped ZnO, the overall increase in power conversion efficiency was due to better ionic radii and more crystalline structure of Sr-doped ZnO. The improvement in the band gap was also attributed to the improvement in the power conversion efficiency of the solar cell.

Sr-doped ZnO nanorods on AAO template as the piezoelectric material for energy harvester show an open circuit voltage of 3–6.4 mV and short circuit current of 0.45–1.5 uA. The addition of Sr in ZnO nanostructures increased the band gap, resulting in an improvement in the voltage and current output of the designed system. Table 4 shows the benchmark comparison of the study with previous research based on ZnO nanostructure for MEMS energy harvesting. The table shows an improved open circuit voltage as compared to other ZnO nanostructures and doped nanostructures. Since the method of fabrication of the substrate and thin film is low, it is more suitable for the generation of mV of energy for small-scale applications.

5 Conclusion

This study presents an investigation into Sr-doped ZnO nanorods utilized as an AAO template for dye-sensitized solar cells and MEMS energy harvesters. Notably, the calculated band gap was found to increase from 3.25 eV in pristine ZnO to 3.27 eV in Sr-doped ZnO, a phenomenon attributed to the incorporation of strontium ions affecting the electronic band structure. The utilization of a porous AAO template facilitated the fabrication of smoother nanorods, owing to the templating effect provided by the uniform pores. These controlled growth conditions resulted in more ordered and uniform nanorod surfaces, enhancing the overall performance of the nanostructures. The subsequent evaluation of the solar cell's efficiency yielded promising results, including a 2.2% conversion efficiency, 0.67 V open circuit voltage, 5.1 mA/cm^2 short circuit current density, and a 0.62 fill factor. When compared to conventional ZnO nanorods, the Sr-doped ZnO nanorods on the AAO template demonstrated significant improvements in power conversion efficiency, primarily due to the reduced band gap, which facilitates efficient electron transport from the dye to the external circuit. Additionally, the porous nature of the AAO template enhanced electron mobility. Furthermore, the MEMS energy harvester exhibited enhanced performance, with open circuit voltages ranging from 7.0 to 7.2 mV and short circuit currents ranging between 1.05 and 1.15 uA for both polarities. These findings underscore the potential of the fabricated film for applications in both solar energy conversion and piezoelectric energy harvesting.

Data availability statement

The raw data supporting the conclusions of this article will be made available by the authors, without undue reservation.

Author contributions

MSA: Conceptualization, Methodology, Software, Validation, Writing–original draft. MWA: Conceptualization, Software, Validation, Writing–review and editing, Supervision, Project

administration. ST: Data curation, Software, Writing–review and editing. MI: Supervision, Validation, Writing–review and editing.

Funding

The authors declare that no financial support was received for the research, authorship, and/or publication of this article.

Acknowledgments

The authors would like to acknowledge the nanoelectronics lab, Department of Electronics, GC University Lahore for providing the facility to carry out the research and experimental work.

Conflict of interest

The authors declare that the research was conducted in the absence of any commercial or financial relationships that could be construed as a potential conflict of interest.

Publisher's note

All claims expressed in this article are solely those of the authors and do not necessarily represent those of their affiliated organizations, or those of the publisher, the editors and the reviewers. Any product that may be evaluated in this article, or claim that may be made by its manufacturer, is not guaranteed or endorsed by the publisher.

References

Afzal, M. J., Javaid, F., Tayyaba, S., Ashraf, M. W., and Hossain, M. K. (2020). "Study on the induced voltage in piezoelectric smart material (PZT) using ANSYS electric & fuzzy logic," in Proceedings of International Exchange and Innovation Conference on Engineering & Sciences (IEICES), Fukuoka City, Japan, October 19-20, 2023.

Akinaga, H. (2020). Recent advances and future prospects in energy harvesting technologies. *Jpn. J. Appl. Phys.* 59, 110201. doi:10.35848/1347-4065/abbfa0

Ali, B., Ashraf, M. W., and Tayyaba, S. (2019). Simulation, fuzzy analysis and development of ZnO nanostructure-based piezoelectric MEMS energy harvester. *Energies* 12, 807. doi:10.3390/en12050807

Alizadeh, A., Roudgar-Amoli, M., Bonyad-Shekalgourabi, S.-M., Shariatinia, Z., Mahmoudi, M., and Saadat, F. (2022). Dye sensitized solar cells go beyond using perovskite and spinel inorganic materials: a review. *Renew. Sustain. Energy Rev.* 157, 112047. doi:10.1016/j.rser.2021.112047

An, Q., Chen, J., Tao, Z., Ming, W., and Chen, M. (2020). Experimental investigation on tool wear characteristics of PVD and CVD coatings during face milling of Ti6242S and Ti-555 titanium alloys. *Int. J. Refract. Metals Hard Mater.* 86, 105091. doi:10.1016/j.ijrmhm.2019.105091

Anand, A., Asok, A., Arpith, P., Sandeep, S., Nandana, G., Panicker, S., et al. (2021). "Optimizing design of wearable energy generator for body motion based energy harvesting," in 2021 5th International Conference on Trends in Electronics and Informatics (ICOEI), Tirunelveli, India, 03-05 June 2021.

Ari, D. A., Sezgin, A., Unal, M., Akman, E., Yavuz, I., Liang, F. C., et al. (2023). Design of an amorphous $ZnWSe_2$ alloy-based counter electrode for highly efficient dye-sensitized solar cells. *Mater. Chem. Front.* 7, 4120–4131. doi:10.1039/d3qm00320e

Baig, F., Ashraf, M. W., Asif, A., and Imran, M. J. O. (2020). A comparative analysis for effects of solvents on optical properties of Mg doped ZnO thin films for optoelectronic applications. *Optik* 208, 164534. doi:10.1016/j.ijleo.2020.164534

Bestley Joe, S., and Shaby, S. M. J. A. N. (2021). Characterization and performance analysis of piezoelectric ZnO nanowire for low-frequency energy harvesting applications. *Appl. Nanosci.* 13, 971–984. doi:10.1007/s13204-021-01964-8

Boing, D., De Oliveira, A. J., and Schroeter, R. B. J. T. I. J. O. A. M. T. (2020). Evaluation of wear mechanisms of PVD and CVD coatings deposited on cemented carbide substrates applied to hard turning. *Int. J. Adv. Manuf. Technol.* 106, 5441–5451. doi:10.1007/s00170-020-05000-x

Bounouh, A., and Bélières, D. (2014). Resonant frequency characterization of MEMS based energy harvesters by harmonic sampling analysis method. *Measurement* 52, 71–76. doi:10.1016/j.measurement.2014.03.013

Castán, J.-M. A., Mwalukuku, V. M., Riquelme, A. J., Liotier, J., Huaulmé, Q., Anta, J. A., et al. (2022). Photochromic spiro-indoline naphthoxazines and naphthopyrans in dye-sensitized solar cells. *Mater. Chem. Front.* 6, 2994–3005. doi:10.1039/d2qm00375a

Chakraborty, S., Li, J., and Bhattacharya, P. J. J. O. P. C. M. (2021). The solution to the global energy crisis with new materials, and sustainability. *J. Phase Change Materials* 1 (2) . doi:10.58256/jpcm.v1i2.17

Cherumannil Karumuthil, S., Rajeev, S. P., and Varghese, S. (2017). Piezo-tribo nanoenergy harvester using hybrid polydimethyl siloxane based nanocomposite. *Nano Energy* 40, 487–494. doi:10.1016/j.nanoen.2017.08.052

Choi, E., Kim, J., Boo, J.-H., and Hong, B. (2015). Synthesis and application of ZnO nanorods using the ultra-thin porous AAO template fabricated by new method. *J. Nanosci. Nanotechnol.* 15, 8395–8400. doi:10.1166/jnn.2015.11476

Chung, J., Lee, J., and Lim, S. (2010). Annealing effects of ZnO nanorods on dye-sensitized solar cell efficiency. *Phys. B Condens. Matter* 405, 2593–2598. doi:10.1016/j.physb.2010.03.041

Davidson, J., and Mo, C. (2014). Recent advances in energy harvesting technologies for structural health monitoring applications. *Smart Mater. Res.* 2014, 1–14. doi:10.1155/2014/410316

Debnath, B., and Kumar, R. J. I. T. O. I. A. (2022). A comparative simulation study of the different variations of pzt piezoelectric material by using A MEMS vibration energy harvester. *Energy Harvest.* 58, 3901–3908. doi:10.1109/tia.2022.3160144

Dobrzański, L., and Pakuła, D. J. J. O. M. P. T. (2005). Comparison of the structure and properties of the PVD and CVD coatings deposited on nitride tool ceramics. *J. Mat. Process. Technol.* 164, 832–842. doi:10.1016/j.jmatprotec.2005.02.094

Esakki, E. S., Vivek, P., and Sundar, S. M. (2023). Influence on the efficiency of dye-sensitized solar cell using Cd doped ZnO via solvothermal method. *Inorg. Chem. Commun.* 147, 110213. doi:10.1016/j.inoche.2022.110213

Esgin, H., Caglar, Y., and Caglar, M. (2022). Photovoltaic performance and physical characterization of Cu doped ZnO nanopowders as photoanode for DSSC. *J. Alloys Compd.* 890, 161848. doi:10.1016/j.jallcom.2021.161848

Fang, H.-B., Liu, J.-Q., Xu, Z.-Y., Dong, L., Wang, L., Chen, D., et al. (2006). Fabrication and performance of MEMS-based piezoelectric power generator for vibration energy harvesting. *Microelectron. J.* 37, 1280–1284. doi:10.1016/j.mejo.2006.07.023

Gullapalli, H., Vemuru, V. S., Kumar, A., Botello-Mendez, A., Vajtai, R., Terrones, M., et al. (2010). Flexible piezoelectric ZnO–paper nanocomposite strain sensor. *Small* 6, 1641–1646. doi:10.1002/smll.201000254

Hodes, G. J. P. C. C. P. (2007). Semiconductor and ceramic nanoparticle films deposited by chemical bath deposition. *Phys. Chem. Chem. Phys.* 9, 2181–2196. doi:10.1039/b616684a

Iqbal, M., Nauman, M. M., Khan, F. U., Abas, P. E., Cheok, Q., Iqbal, A., et al. (2021). Vibration-based piezoelectric, electromagnetic, and hybrid energy harvesters for microsystems applications: a contributed review. *Int. J. Energy Res.* 45, 65–102. doi:10.1002/er.5643

Karumuthil, S. C., Rajeev, S. P., and Varghese, S. (2019). Poly(vinylidene fluoride-trifluoroethylene)-ZnO nanoparticle composites on a flexible poly(dimethylsiloxane) substrate for energy harvesting. *ACS Appl. Nano Mater.* 2, 4350–4357. doi:10.1021/acsanm.8b02248

Liu, H., Lee, C., Kobayashi, T., Tay, C. J., and Quan, C. (2012). Piezoelectric MEMS-based wideband energy harvesting systems using a frequency-up-conversion cantilever stopper. *Sensors Actuators A Phys.* 186, 242–248. doi:10.1016/j.sna.2012.01.033

Maamer, B., Boughamoura, A., Fath El-Bab, A. M. R., Francis, L. A., and Tounsi, F. (2019). A review on design improvements and techniques for mechanical energy harvesting using piezoelectric and electromagnetic schemes. *Energy Convers. Manag.* 199, 111973. doi:10.1016/j.enconman.2019.111973

Mahdhi, H., Djessas, K., and Ayadi, Z. B. J. M. L. (2018). Synthesis and characteristics of Ca-doped ZnO thin films by rf magnetron sputtering at low temperature. *Mat. Lett.* 214, 10–14. doi:10.1016/j.matlet.2017.11.108

Md Ralib, A. A., Nordin, A. N., Salleh, H., and Othman, R. (2012). Fabrication of aluminium doped zinc oxide piezoelectric thin film on a silicon substrate for piezoelectric MEMS energy harvesters. *Microsyst. Technol.* 18, 1761–1769. doi:10.1007/s00542-012-1550-9

Michalska-Domańska, M., Norek, M., Stępniowski, W. J., and Budner, B. (2013). Fabrication of high quality anodic aluminum oxide (AAO) on low purity aluminum—a comparative study with the AAO produced on high purity aluminum. *Electrochimica Acta* 105, 424–432. doi:10.1016/j.electacta.2013.04.160

Mugle, D., and Jadhav, G. (2016). Short review on chemical bath deposition of thin film and characterization. *AIP Conf. Proc.* 1728, 020597. doi:10.1063/1.4946648

Mujahid, M., and Al-Hartomy, O. A. (2023). Fabrication and synthesis of dye-sensitized solar cells (DSSC) using Pd doped ZnO photoanodes and extract of plant leaves as a natural dye. *Mater. Res. Innovations* 27, 194–203. doi:10.1080/14328917.2022.2113270

Pastuszak, J., and Węgierek, P. (2022). Photovoltaic cell generations and current research directions for their development. *Mater. (Basel)* 15, 5542. doi:10.3390/ma15165542

Poon, K. K., Schafföner, S., Einarsrud, M.-A., and Glaum, J. J. J. O. T. E. C. S. (2021). Barium titanate-based bilayer functional coatings on Ti alloy biomedical implants. *J. Eur. Ceram. Soc.* 41, 2918–2922. doi:10.1016/j.jeurceramsoc.2020.12.023

Rajeev, S. P., John, N., Nair, S., Ashfak, A., Prabha, S., Nimmy, C., et al. (2021). Nature-inspired PDMS cumulonimbus micro-energy-harvesting cloud. *Appl. Nanosci.* 11, 3. doi:10.1007/s13204-020-01556-y

Rajeev, S. P., Sivapriya, S., Cherumannil Karumuthil, S., and Varghese, S. (2020). Prototype of energy harvesting door handles using polymer nanocomposite. *Appl. Nanosci.* 10, 1–13. doi:10.1007/s13204-019-01027-z

Rathnasekara, R., and Hari, P. (2022). Enhancing the efficiency of dye-sensitized solar cells (DSSCs) by nanostructured Ag-doped ZnO electrodes. *ChemistrySelect* 7, e202200830. doi:10.1002/slct.202200830

Richhariya, G., Meikap, B. C., and Kumar, A. (2022). Review on fabrication methodologies and its impacts on performance of dye-sensitized solar cells. *Environ. Sci. Pollut. Res.* 29, 15233–15251. doi:10.1007/s11356-021-18049-2

Sarwar, G., and Ashraf, M. W. (2020). Parametric estimation of Group II element doped zinc oxide nanostructures using fuzzy logic. *J. Intelligent Fuzzy Syst.* 38, 5865–5875. doi:10.3233/jifs-179674

Sarwar, G., Oad, A., Bibi, R., Ashraf, M. W., Tayyaba, S., and Akhlaq, M. (2021). Simulation, synthesis and band-gap engineering of 2nd group doped ZnO nanostructures. *Mater. Res. Express* 8, 085004. doi:10.1088/2053-1591/ac17aa

Selva Esakki, E., Vivek, P., Devi, L. R., Sarathi, R., Sheeba, N. L., and Sundar, S. M. (2022). Influence on electrochemical impedance and photovoltaic performance of natural DSSC using *Terminalia catappa* based on Mg-doped ZnO photoanode. *J. Indian Chem. Soc.* 99, 100756. doi:10.1016/j.jics.2022.100756

Sheikh, N., Afzulpurkar, N., and Ashraf, M. W. J. J. O. N. (2013). Robust nanogenerator based on vertically aligned ZnO nanorods using copper substrate. *J. Nanomater.* 2013, 1–8. doi:10.1155/2013/861017

Singh, S. S., and Shougaijam, B. (2022). "Recent development and future prospects of rigid and flexible dye-sensitized solar cell: a review," in *Contemporary trends in semiconductor devices: theory, experiment and applications*. Editors R. Goswami and R. Saha (Singapore: Springer Nature Singapore).

Sun, H., Yin, M., Wei, W., Li, J., Wang, H., and Jin, X. J. M. T. (2018). MEMS based energy harvesting for the Internet of Things: a survey. *Microsyst. Technol.* 24, 2853–2869. doi:10.1007/s00542-018-3763-z

Tao, K., Yi, H., Tang, L., Wu, J., Wang, P., Wang, N., et al. (2019). Piezoelectric ZnO thin films for 2DOF MEMS vibrational energy harvesting. *Surf. Coatings Technol.* 359, 289–295. doi:10.1016/j.surfcoat.2018.11.102

Tayyaba, S., Ashraf, M. W., Tariq, M. I., Akhlaq, M., Balas, V. E., Wang, N., et al. (2020). Simulation, analysis, and characterization of calcium-doped ZnO nanostructures for dye-sensitized solar cells. *Energies* 13, 4863. doi:10.3390/en13184863

Tiwari, B., Babu, T., and Choudhary, R. J. M. T. P. (2021). Piezoelectric lead zirconate titanate as an energy material: a review study. *A Rev. study* 43, 407–412. doi:10.1016/j.matpr.2020.11.692

Toshiyoshi, H., Ju, S., Honma, H., Ji, C.-H., and Fujita, H. (2019). MEMS vibrational energy harvesters. *Sci. Technol. Adv. Mater.* 20, 124–143. doi:10.1080/14686996.2019.1569828

Vaseem, M., Umar, A., and Hahn, Y. B. (2010). "ZnO nanoparticles: growth, properties, and applications," in *Metal oxide nanostructures and their applications* (American Scientific Publishers), 10–20.

Vijayan, T., Chandramohan, R., Valanarasu, S., Thirumalai, J., and Subramanian, S. (2008). Comparative investigation on nanocrystal structure, optical, and electrical properties of ZnO and Sr-doped ZnO thin films using chemical bath deposition method. *J. Mater. Sci.* 43, 1776–1782. doi:10.1007/s10853-007-2404-1

Wang, P., and Du, H. (2015a). ZnO thin film piezoelectric MEMS vibration energy harvesters with two piezoelectric elements for higher output performance. *Rev. Sci. Instrum.* 86, 075002. doi:10.1063/1.4923456

Wang, P., and Du, H. (2015b). ZnO thin film piezoelectric MEMS vibration energy harvesters with two piezoelectric elements for higher output performance. *Rev. Sci. Instrum.* 86, 075002. doi:10.1063/1.4923456

Wasim, M. F., Tayyaba, S., Ashraf, M. W., and Ahmad, Z. J. S. (2020). Modeling and piezoelectric analysis of nano energy harvesters. *Sensors (Basel)* 20, 3931. doi:10.3390/s20143931

Wu, J. J., and Liu, S. C. J. A. M. (2002). Low-temperature growth of well-aligned ZnO nanorods by chemical vapor deposition. *Adv. Mat.* 14, 215–218. doi:10.1002/1521-4095(20020205)14:3<215::aid-adma215>3.0.co;2-j

Yarahmadi, M., Maleki-Ghaleh, H., Mehr, M. E., Dargahi, Z., Rasouli, F., and Siadati, M. H. (2021). Synthesis and characterization of Sr-doped ZnO nanoparticles for photocatalytic applications. *J. Alloys Compd.* 853, 157000. doi:10.1016/j.jallcom.2020.157000

Yuliasari, F., Aprilia, A., and Hidayat, R. (2022). Improved dye-sensitized solar cell performance with hedgehog-like shaped ZnO nanorods grown using ZnO nanoparticles seed layer. *Mater. Today Proc.* 52, 248–251. doi:10.1016/j.matpr.2022.02.193

Zhang, C., Fan, W., Wang, S., Wang, Q., Zhang, Y., and Dong, K. (2021). Recent progress of wearable piezoelectric nanogenerators. *ACS Appl. Electron. Mater.* 3, 2449–2467. doi:10.1021/acsaelm.1c00165

Zhao, X., Li, S., Ai, C., Liu, H., and Wen, D. (2019). Fabrication and characterization of the Li-doped ZnO thin films piezoelectric energy harvester with multi-resonant frequencies. *Micromachines* 10, 212. doi:10.3390/mi10030212

Zhou, X., Liu, G., Han, B., and Liu, X. (2021). Different kinds of energy harvesters from human activities. *Int. J. Energy Res.* 45, 4841–4870. doi:10.1002/er.6045

Zorlu, Ö., and Külah, H. J. S. (2013). A MEMS-based energy harvester for generating energy from non-resonant environmental vibrations. *Sensors Actuators A Phys.* 202, 124–134. doi:10.1016/j.sna.2013.01.032